First-principles investigation of electrochemical dissolution of Pt nanoparticles and kinetic simulation

Cite as: J. Chem. Phys. **151**, 234711 (2019); https://doi.org/10.1063/1.5129631
Submitted: 02 October 2019 . Accepted: 29 November 2019 . Published Online: 17 December 2019

Jing Zhu, Sulei Hu, Zhenhua Zeng, and Wei-Xue Li

The Journal of Chemical Physics ARTICLE scitation.org/journal/jcp

First-principles investigation of electrochemical dissolution of Pt nanoparticles and kinetic simulation

Cite as: J. Chem. Phys. 151, 234711 (2019); doi: 10.1063/1.5129631
Submitted: 2 October 2019 • Accepted: 29 November 2019 •
Published Online: 17 December 2019

Jing Zhu,[1] Sulei Hu,[1,2] Zhenhua Zeng,[3] and Wei-Xue Li[1,2,a)]

AFFILIATIONS

[1]Department of Chemical Physics, School of Chemistry and Materials Science, iCHeM, CAS Excellence Center for Nanoscience, University of Science and Technology of China, Hefei 230026, Anhui, China
[2]Hefei National Laboratory for Physical Sciences at Microscale, Hefei 230026, Anhui, China
[3]Davidson School of Chemical Engineering, Purdue University, West Lafayette, Indiana 47907, USA

Note: This paper is part of the JCP Special Topic Collection on Catalytic Properties of Model Supported Nanoparticles.
[a)]**Electronic mail:** wxli70@ustc.edu.cn

ABSTRACT

Dissolution is the primary route of Pt nanoparticle degradation in electrochemical devices, e.g., fuel cells. Investigation of potential-dependent dissolution kinetics of Pt nanoparticles is crucial to optimize the nanoparticle size and operating conditions for better performance. A mean-field kinetic theory under the steady-state approximation, combined with atomistic thermodynamics and Wulff construction, was developed to study the interplay between oxygen chemisorption, electrode potential, and particle size on the dissolution of Pt nanoparticles. We found that although oxygen chemisorption from electrode potential-induced water splitting can stabilize Pt nanoparticles through decreasing the surface energy and increasing the redox potential, the electrode potential plays a more decisive role in facilitating the dissolution of Pt nanoparticles. In comparison with the minor effect of oxygen chemisorption, an increase in the particle size, though reducing the dispersion, has a more significant effect on the suppression of the dissolution. These theoretical understandings on the effects of electrode potential and particle size on the dissolution are crucial for optimizing the nanoparticle size under oxidative operating conditions.

I. INTRODUCTION

The highly dispersed metal Pt nanoparticles (NPs) supported on the conductive support are intensively studied as catalysts in polymer electrolyte fuel cells and electrolysis cells. Among others, the degradation of Pt NPs due to mass loss and particle coarsening restricts seriously its large-scale applications.[1–5] Experimentally, it was found that the electrode potential, alloying, support, temperature, and particle size significantly affected the degradation rate of Pt NPs.[6–13] Unraveling the degradation mechanisms[13–16] and evaluating their dependence on these involved factors of Pt electrocatalysts[17–19] using, for instance, computational investigation, is important to improve their overall performance and particular stability under the operational condition.[20–26]

The metal NPs electrochemical dissolution and redeposition kinetics have been studied based on the Lifshitz-Slyozov-Wagner (LSW) theory[27] and the Butler-Volmer equation.[28–32] It was found that the ratio of the dissolution rate to deposition rate is directly dependent on the electrode potential, which determines eventually the overall durability. It has been found that the Pt NPs are gradually oxidized with an increase in the electrode potential.[33–36] With the adsorption of oxygen from water splitting and even the formation of Pt oxide covering Pt NPs, the electrochemical dissolution changed.[35] Since the corresponding dissolution process toward the Pt^{2+} ions could be slow, the formation of oxide was thought to passivate the metal surfaces. Nevertheless, it remains unclear how the electrode potential affects the oxygen adsorption and oxidation as well as subsequent electrochemical dissolution.

To investigate the effect of oxygen chemisorption and/or surface oxidation on dissolution of metal NPs, a kinetic theory based on the Butler-Volmer equation considering the electrode potential influence was formulated.[29,30] The oxygen coverage or Pt activity in Pt-PtO_x solutions formed, representing the percentage of metallic Pt to dissolve galvanically, was suggest to play an important role, though oxygen coverage or Pt activity as well as their dependence on the electrode potential is largely unknown. Alternatively, they were extracted by fitting the evolution curve of the electrochemical active area loss,[37] a fact of that prevents microscopic understanding and rational design of stable electrocatalysts. It is important to investigate the relationship of the electrode potential with the chemisorption of oxygen and formation of oxide. Since the oxygen chemisorption and/or oxide formation not only change the surface energy of the metal NPs but also the redox potential of dissolution/deposition, a kinetic dissolution theory taking into account consistently all these factors in addition to the particle size is, therefore, highly desirable.

In our previous works, we developed a first-principles mean-field kinetic theory based on the LSW framework and steady-state approximation to provide a generic and atomistic description of Ostwald ripening and disintegration of supported metal NPs for gas-solid phase reaction.[38–40] Here, we extend the kinetic theory to describe the dissolution of the metal NPs under electrochemical conditions, where the effects of the electrode potential, oxygen chemisorption, oxidation, and particle size are described consistently. In particular, the influence of the oxygen chemisorption and oxide formation on the surface energy and redox potential of the metal NPs as well as their dependence on the electrode potential was addressed based on *ab initio* thermodynamics.[41–45] The morphology effect of the Pt NPs was approximated by utilizing the Wulff construction and potential-dependent surface energies of Pt(111) and Pt(100). The present study of electrochemical dissolution at a wide range of electrode potentials and particle sizes provides atomistic insights for the optimization of Pt nanocatalysts with balanced stability and activity.

II. THEORETICAL FRAMEWORK

A. Rate equation of deposition and dissolution

The elementary processes under electrochemical conditions contain the galvanic dissolution and deposition of metal atom/ion through the electrolyte. The kinetic simulation is based on the conservation of metal mass by including both residual NPs and dissolved ions. The galvanic deposition rate v_d of the half-reaction (ions + ne^- → metal) is a function of the ion concentration c and electrode potential U, which can be expressed by the Butler-Volmer equation (partial parameters defined in Table I, k_B is the Boltzmann constant) as

$$v_d = k^0 c \exp\left[-\frac{(1-\beta)n(U-\varphi^0)}{k_B T}\right]. \quad (1)$$

For reference, the equilibrium ion concentration of bulk metal $c_{eq}(\infty)$ as a function of electrode potential based on the Nernst equation (c^0 as the concentration reference of 1 mol/l) is

$$c_{eq}(\infty) = c^0 \exp\left[\frac{n(U-\varphi^0)}{k_B T}\right]. \quad (2)$$

TABLE I. Parameters and constants used in dissolution/deposition equations of metal Pt without mention otherwise.

Parameters	Values	Unit
Standard rate constant k^0	2×10^{-11}	cm/s
Anodic transfer factor β	0.5 (28)	
Electron number n	2	
Standard redox potential φ^0	1.188 (28)	V
Temperature T	353	K
H^+ concentration c_{H^+}	1	mol/l
Surface energy γ	0.155 (61)	eV/Å^2
Atomic molar volume Ω	15 (46)	Å^3
Contact angle α	90 (60)	deg

For a given particle with the curvature radius of R and surface free energy γ, the corresponding chemical potential shift per atom with respect to the bulk counterpart, which could be described approximately by the Gibbs-Thomson equation, $\Delta\mu(R)$, is written as

$$\Delta\mu(R) = \frac{2\gamma\Omega}{R}. \quad (3)$$

We note that the surface energy in the above equation could be morphology[38,39,46] and size[47,48] dependent. Through the thermodynamic analysis of the reaction (ions + ne^- → metal) that associates μ (dependent on R) with the Gibbs free energy change and φ^0 (relevant to c_{eq}), the ion concentration in equilibrium for a finite size metal particle is, therefore, written as

$$c_{eq}(R) = c_{eq}(\infty) \exp\left[\frac{\Delta\mu(R)}{k_B T}\right]. \quad (4)$$

Under the steady state, the ion concentration on the surface of a particle is assumed to be equal to the equilibrium concentration at a given electrode potential. The net ion deposition rate would depend on the difference of ion concentration between that on the particle surface and that in solution as shown in Fig. 1, where the ions distribute evenly in solution.

Combining Eqs. (1), (2), and (4), the electrochemical ion deposition rate of the particle surface as a function of the R could be written as

$$v_d(R) = c^0 k^0 \exp\left[\frac{\beta n(U-\varphi^0)}{k_B T}\right] \exp\left[\frac{\Delta\mu(R)}{k_B T}\right]. \quad (5)$$

Considering NPs in the form of a spherical segment on a flat support as shown in Fig. 1, a contact angle α was used. The volume and area of this segment are $4\pi R^3\alpha_1/3$ and $4\pi R^2\alpha_2$, respectively, where $\alpha_1 = (2 - 3\cos\alpha + \cos^3\alpha)/4$ and $\alpha_2 = (1 - \cos\alpha)/2$.[5]

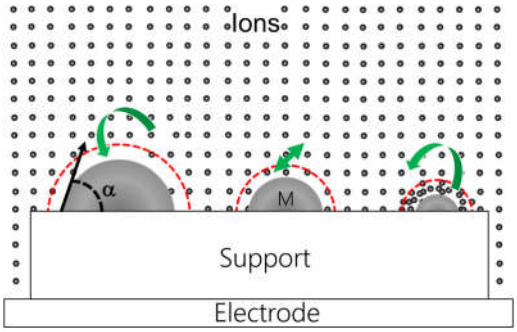

FIG. 1. Schematic of the distribution of ions on the surface (in red cycle) of metal NPs and in electrolyte solution.

The net deposition current J of an individual particle could be written as

$$J(R) = 4\pi R^2 \alpha_2 \left[v_d(R^*) - v_d(R) \right], \tag{6}$$

where the critical radius R^* is the radius of a "virtual" particle, which is in equilibrium with the ion concentration in solution, and varies during the entire NPs evolution process. We note that R^* is dependent on the overpotential $U - \varphi^0$, temperature, and surface energy, respectively. For a system with rather low ion concentration, for example, an open system, the corresponding R^* would be considerably large. Since the typical particle size in solution is modest, this means that in this particular case, $J(R)$ would always have a negative sign and the corresponding net process is a dissolution process.

The particle volume change related to the net deposition current is given as

$$\frac{d}{dt}\left(\frac{4}{3}\pi R^3 \alpha_1\right) = 4\pi R^2 \alpha_1 \frac{dR}{dt} = J\Omega. \tag{7}$$

As a result, combining Eqs. (6) and (7), the growth rate dR/dt of an individual particle becomes

$$\frac{dR}{dt} = \Omega \frac{\alpha_2}{\alpha_1} \left[v_d(R^*) - v_d(R) \right], \tag{8}$$

and combining Eqs. (5) and (8), it could be written as

$$\frac{dR}{dt} = P \exp\left[Q\left(U - \varphi^0 \right) \right] \left(\exp\left[\frac{\Delta\mu(R^*)}{k_B T} \right] - \exp\left[\frac{\Delta\mu(R)}{k_B T} \right] \right), \tag{9}$$

where $P = \Omega(\alpha_2/\alpha_1)c^0 k^0$ and $Q = (\beta n)/(k_B T)$.

B. Adsorption-influenced dissolution/deposition

In the electrochemical conditions, the potential-induced water splitting might happen and dissociated oxygenates adsorb and even oxidize the metal surfaces. The corresponding Gibbs surface free energy decreases, and the metal NPs are stabilized. Here, using adsorbed oxygen atoms on a Pt surface as an example, the effective surface energy $\bar{\gamma}$ at a given electrode potential U with the oxygen coverage θ could be calculated by the density functional theory (DFT) as (the symbol with the bar represents the variables in the presence of oxygen)

$$\bar{\gamma}(U,\theta) = \gamma + \Delta\gamma(U,\theta) = \gamma + \theta \Delta G^{ad}(U,\theta), \tag{10}$$

where γ is clean surface energy.

$\Delta\gamma$ is the adsorption free surface energy equal to the product of the adsorbate coverage θ and the corresponding average adsorption Gibbs free energy $\Delta G^{ad}(U,\theta)$,

$$\theta = n_O/A, \tag{11}$$

$$\Delta G^{ad}(U,\theta) = (1/n_O) \times \left(E_{O/slab} - E_{slab} \right) + E_{H_2} - E_{H_2O} + E_c - 2U, \tag{12}$$

where n_O is the number of adsorbed oxygen atoms in the supercell and A is the surface area of the supercell. $E_{O/slab}$ and E_{slab} are the total energy of oxygen adsorbed and clean surfaces, respectively. The correction energy E_c between the total energy and Gibbs free energy includes the zero-point energy (ZPE), integrated heat capacities (δH), entropy effect (TS), and an empirical shift of 0.35 eV per adsorbed oxygen atom.[49] For H_2 gas and water, ZPE, δH, and TS are obtained from the standard thermodynamic table, and for adsorbed oxygen atoms, the corresponding data are calculated from vibrational frequencies within the harmonic approximation.

Considering the NPs exposed different facets i with the ratio of f_i over the whole surface area, which is potential-dependent, the effective surface energy of metal NPs with adsorbates could be rewritten as

$$\bar{\gamma} = \sum_i \bar{f}_i \times \bar{\gamma}_i. \tag{13}$$

Besides the variation of surface energy of the metal NPs, oxygen adsorption also changed the thermodynamics of the surface dissolution and deposition reactions, which is described equivalently here to the standard redox potential of $Pt^{2+} + 2e^- = Pt$ as

$$\Delta G_{Pt^{2+}/Pt} = -2\varphi^0_{Pt^{2+}/Pt}. \tag{14}$$

Due to water splitting induced by the electrode potential, there are oxygens formed on the Pt surface,

$$Pt + xH_2O = Pt\text{-}xO + 2xH^+ + 2xe^-, \tag{15}$$

where x is ratio of the number of the oxygen atoms to the surface Pt atoms. The corresponding reaction Gibbs free energy and the standard redox potential of Eq. (15) could be written as

$$\Delta G_{Pt-xO/Pt} = -2x\varphi^0_{Pt-xO/Pt}. \tag{16}$$

Once oxidative specie Pt-xO formed, it would dissolve to solution, rather than that of Pt,

$$Pt\text{-}xO + 2xH^+ = xH_2O + Pt^{2+} + 2xe^-. \tag{17}$$

The corresponding reaction Gibbs free energy and the standard redox potential could be written as

$$\Delta G_{Pt^{2+}/Pt-xO} = -2x\varphi^0_{Pt^{2+}/Pt-xO}. \tag{18}$$

The standard redox potential of dissolution and deposition of Pt^{2+}/Pt–xO could be derived via

$$\varphi^0_{Pt^{2+}/Pt-xO} = \frac{\varphi^0_{Pt^{2+}/Pt} - x\varphi^0_{Pt-xO/Pt}}{1-x}. \quad (19)$$

In a word, the adsorbate effect on the dissolution and deposition processes is assumed through the reaction of $Pt^{2+}/Pt–xO$. In addition, considering the equilibrium ion concentration of infinite NPs with oxygen adsorption also dependent on the H^+ concentration in solution, Eq. (2) could be rewritten as

$$c_{eq}(\infty) = c^0(c_{H^+}/c^0)^{2x}\exp\left[\frac{n(U-\varphi^0)}{k_BT}\right]. \quad (20)$$

The transfer electron number changes as

$$n = 2(1-x)\beta. \quad (21)$$

Combining Eqs. (20), (21), and (9), the rate equation of an individual Pt particle in the presence of oxygen adsorption can be rewritten as

$$\frac{dR}{dt} = P\exp\left[Q\left(U-\varphi^0_{Pt^{2+}/Pt-xO}\right)\right]\left(\exp\left[\frac{\Delta\bar{\mu}(R^*)}{k_BT}\right]-\exp\left[\frac{\Delta\bar{\mu}(R)}{k_BT}\right]\right), \quad (22)$$

where $P = \Omega(\alpha_2/\alpha_1)c^0(c_{H^+}/c^0)^{2x}k^0$ and $Q = [2(1-x)\beta]/(k_BT)$.

C. Computational details

The energetic data of the surface adsorption on various structures (details in the supplementary material) were performed with the code Vienna *Ab Initio* Simulation Package (VASP.5.4.1),[50,51] using the projected augmented wave (PAW) method.[52,53] Self-consistent total energies are evaluated using the exchange-correlation functions PBE (Perdew, Burke, Ernzerhof).[54] The clean Pt(111) and Pt(100) surfaces and the corresponding oxygen-adsorbed structures were all modeled using an eight-layer (2 × 2) and (3 × 3) slab with the bottom four layers fixed and at least 15 Å of vacuum perpendicular to the slab surface. A cutoff energy of 400 eV and a k-point grid of (7 × 7 × 1) and (5 × 5 × 1) were used for the plane wave expansion and Brillouin zone integration, respectively. The maximum atomic forces are smaller than 0.02 eV/Å, and a total energy was convergence of 10^{-5} eV for the electronic self-consistent field loop. The average adsorption Gibbs free energy per oxygen atom ΔG^{ad} was calculated using water and hydrogen as reference.

III. RESULTS AND DISCUSSION

A. Phase diagram under different electrode potentials

The Gibbs free energy ΔG of oxidative dissolution to Pt^{2+} and bulk oxidation of Pt to PtO and PtO_2 was calculated based on the standard redox potentials (Table S1 in the supplementary material). The results are shown in Fig. 2(a) as a function of the electrode potential U (calculation details in the supplementary material). As the U increases, the calculated ΔG decreases accordingly, indicating that the formation of bulk oxide becomes more and more favorable. When the potential is larger than 0.98 and 1.04 V, the corresponding ΔG becomes exothermic and the formation of bulk PtO and PtO_2 is thermodynamically more stable than that of the Pt metal. On the other hand, the equilibrium potential of Pt^{2+}/Pt is 1.188 V at 1 mol/L and would decrease ~30 mV with per order of magnitude decrease in the Pt^{2+} concentration, according to Eq. (S7) in the supplementary material. When the Pt^{2+} concentration is as low as 1.5×10^{-15} mol/l, the corresponding equilibrium potential becomes 0.75 V.

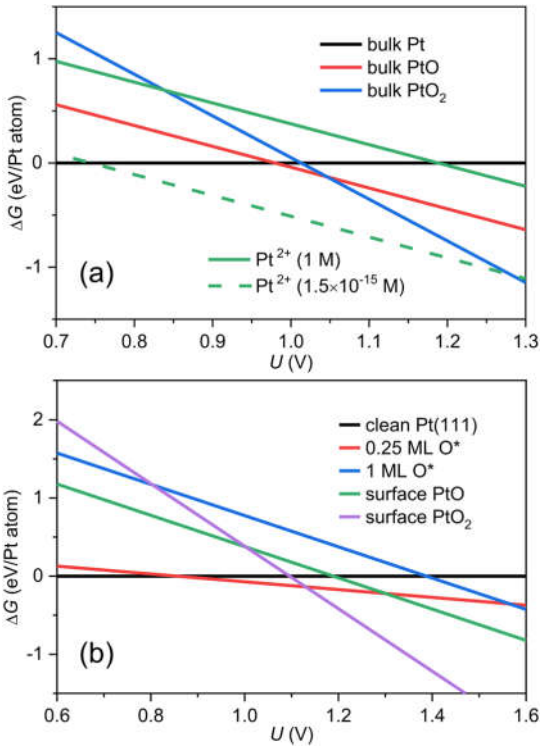

FIG. 2. Phase diagrams under the pressure of 1 bar and the temperature of 298 K. (a) Bulk metal and oxides. (b) Clean and oxygen adsorbed Pt(111) surfaces and the corresponding surface oxides.

To study the surface processes before or during bulk oxidation, using the Pt(111) surface as an example, the surface diagram including oxygen adsorption and surface oxide[55] formation is presented in Fig. 2(b). The standard redox potential of 0.25 ML oxygen on the Pt(111) is 0.85 V, which is 0.14 V lower than that of bulk oxidation. The equilibrium potential of 1 ML oxygen adsorption, surface PtO and PtO_2 is 1.5 V, 1.3 V, and 1.1 V, respectively, indicating that surface PtO_2 oxide would be formed at a relatively lower potential. From a kinetic point of view, to form PtO_2, certain transient states with lower oxygen coverages and oxidized states, for instance, the 1 ML oxygen adsorption and surface PtO, are prerequisites. In this context, larger potentials of 1 ML oxygen and PtO than that of PtO_2 indicates an additional kinetic barrier for the formation of bulk oxide, as found indeed in experiments.[56,57] Considering the kinetics limitation of the formation of bulk and surface oxides, we focus below the oxygen chemisorption up to 1 ML and the corresponding influence on dissolution for the electrode potential varying from 0.75 to 1.15 V.

To study the effect of oxygen chemisorption on dissolution and deposition of Pt NPs, we considered oxygen adsorption on both Pt (111) and (100) surfaces, two dominated facets exposed in Pt NPs.[58] Based on the surface phase diagram at 353 K (see Fig. S5 of the supplementary material), the clean surfaces are more favorable at a low potential. As the electrode potential increases, the (111) and (100) surfaces with 1/4 ML and 1/2 ML oxygen adsorption become more favorable than those of the corresponding clean surfaces at the potentials 0.80 V and 0.81 V, respectively. These oxygen coverages remain until 1.17 V and 1.29 V for the (111) and (100) surface, respectively. The favorable oxygen adsorption is accompanied with decreasing surface energy, depending on the electrode potential as shown in Fig. 3(a). For example, the surface energy of clean Pt(111) was calculated to be 93 meV/Å^2 and decreased to 81 meV/Å^2 and 67 meV/Å^2 at the potentials 0.95 V and 1.15 V, respectively. We had used the calculated surface energies of Pt (111) and (100) surfaces to construct the morphology of Pt NPs based on the Wulff construction [see Fig. 3(b)]. As there is a decrease in the surface energy of both facets by oxygen adsorption, the shape of Pt NPs does not have a substantial change in the potential range of 0.75 V–1.15 V. Specifically, the particle is dominantly enclosed by the (111) facet, but the ratio of the (100) facet increased from 18% at 0.75 V to 34% at 1.15 V (see Table S5 of the supplementary material). Along with the evolution of surface energies and the ratio of each facet, the effective surface energies of NPs, which are a weighted average of the surface energy and the ratio of the facet, decrease from 96 meV/Å^2 to 86 meV/Å^2 and 69 meV/Å^2 at 0.95 V and 1.15 V [see Fig. 3(c)], respectively. The decreasing surface energy indicates that the Pt NPs are gradually stabilized at higher electrode potentials.

In addition to the decrease in the surface energy, adsorption of oxygen atoms also increases the equilibrium potential of Pt dissolution. Based on the surface phase diagram at 298 K (see Fig. S6 of the supplementary material), the redox coupling of deposition and dissolution reactions changes from Pt^{2+}/Pt to Pt^{2+}/Pt(111)-p(2 × 2)-1O and Pt^{2+}/Pt(100)-c(2 × 2)-2O, respectively, at the potential over ~0.85 V. Considering the standard redox potential of Pt^{2+}/Pt is 1.188 V for both Pt (111) and (100) facets, the standard redox potentials of Pt^{2+}/Pt(111)-p(2 × 2)-1O and Pt^{2+}/Pt(100)-c(2 × 2)-2O were calculated to be 1.314 V and 1.546 V, respectively. The increasing redox potential of dissolution and deposition reactions indicates that the equilibrium concentration of NPs decreases at a given potential and oxygen adsorption tends to prevent the dissolution. In kinetic simulations below, we will demonstrate that both the lowered surface energy and especially the increasing redox potential slow considerably the metal NPs dissolution.

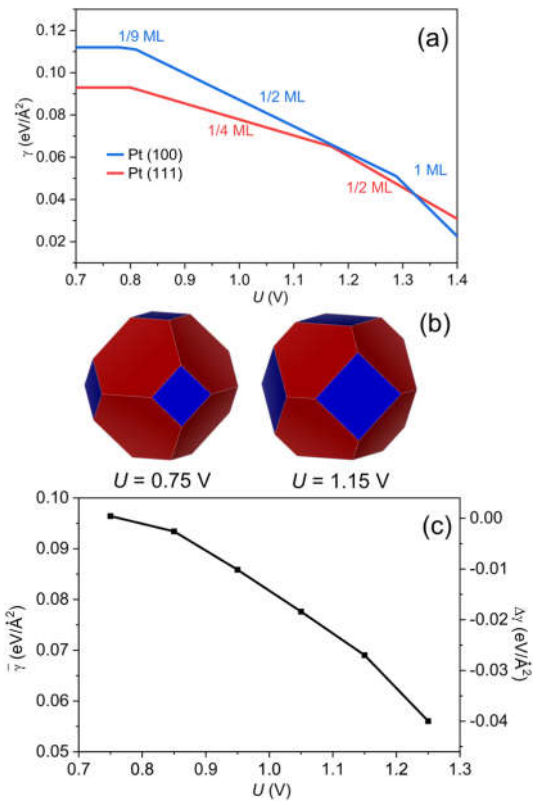

FIG. 3. (a) Surface energy γ as a function of electrode potential U of Pt(111) and Pt(100) facets. (b) Pt morphology from the Wulff construction based on the surface energies by DFT calculations under different U. (c) Effective surface energy and its change as a function of U.

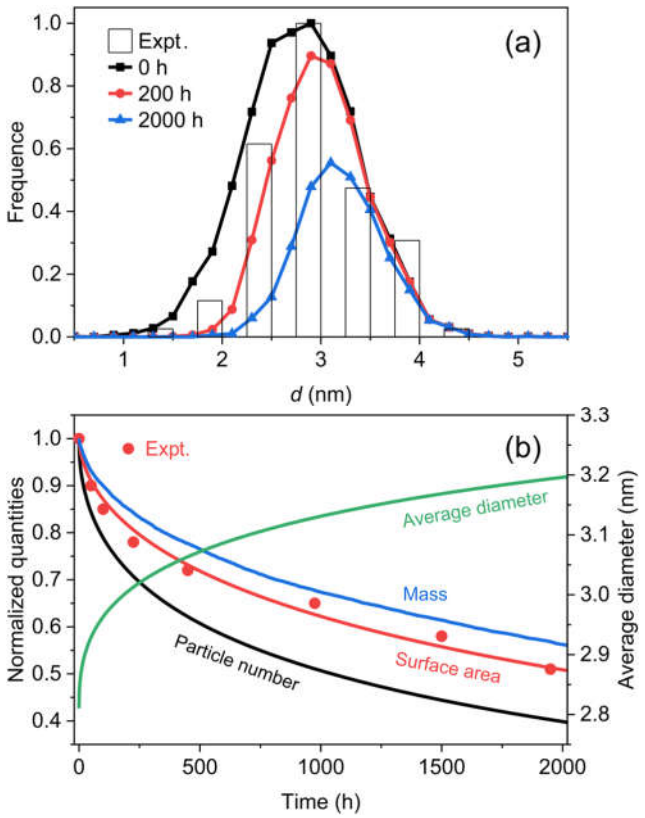

FIG. 4. (a) Initial particle size distribution (PSD) from the experiment with the normal distribution of the average particle diameter of 2.8 nm, and the relative standard deviation σ of 0.2 and subsequent evolution of dissolution at 0.75 V. (b) Evolution of the normalized surface area, particle number, total mass, and average diameter of the residual NPs.

B. Kinetics of electrochemical dissolution

The parameters and their values used in the simulation are presented in Table I. The initial particle size distribution (PSD) from the experiment is shown in Fig. 4(a), a normal distribution with the average diameter of 2.8 nm and a relative standard deviation of 0.2.[59] The contact angle indicates the interaction strength between the Pt nanoparticles and carbon support and could change from 20° to 90° for the various carbon supports, which was assumed to be 90° in all the following kinetic simulations.[60] For smaller contact angles (stronger metal-support interaction), the supported NPs are stabilized and the tendency of dissolution is weakened.[11] For the clean Pt surface, the experimental surface energy of 155 meV/Å^2 is used.[61] The standard rate constant k^0 of 2×10^{-11} cm/s is an empirical parameter extracted by fitting the experimental surface area loss at 0.75 V, a typical potential of the fuel-cell operation as shown in Fig. 4(b). The changes of surface energy and standard redox potential due to oxygen adsorption were derived from the above DFT calculations.

In comparison with the slopes of the normalized quantity evolution curves, the surface area loss is faster than the mass loss, accompanied by the more sharp decrease in the particle number. The average diameter of the PSD gradually increases from 2.8 nm to 3.2 nm after 2000 h. The increase in the average diameter is because of the faster dissolution of smaller NPs than that of the larger ones, different from the growth of the larger one at the expense of the smaller one for Ostwald ripening.[40,62] Indeed, the evolution of the PSD from 0 to 200 and then to 2000 h [see Fig. 4(a)] shows that the decrease in the particle number occurs mainly for the smaller ones, whereas the particle number for the size larger than, in particular, 3.5 nm hardly decreases. The results indicate that there is a net dissolution under the experimental condition considered.

As discussed above, the adsorbed oxygen atoms lower the corresponding surface energies and increase the standard redox potentials, stabilizing the metal NPs and suppressing the dissolution. We now quantify this passivation effect on the overall dissolution kinetics at 1.15 V [Fig. 5(a)]. At such a potential, it only takes 0.02 h to lose 80% of the initial surface area if these effects are not considered, i.e., using the same parameters as those used in the above simulation

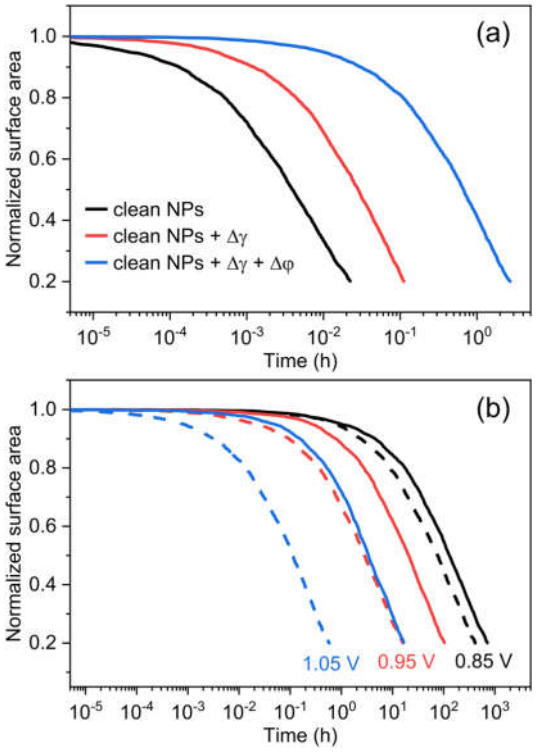

FIG. 5. (a) Surface area loss curves of clean NPs and considering changes in the surface energy and standard redox potential at 1.15 V. (b) Surface area loss curves at various electrode potentials. Dashed lines—clean NPs. Solid lines—considering the total effect of changes in the surface energy and standard redox potential.

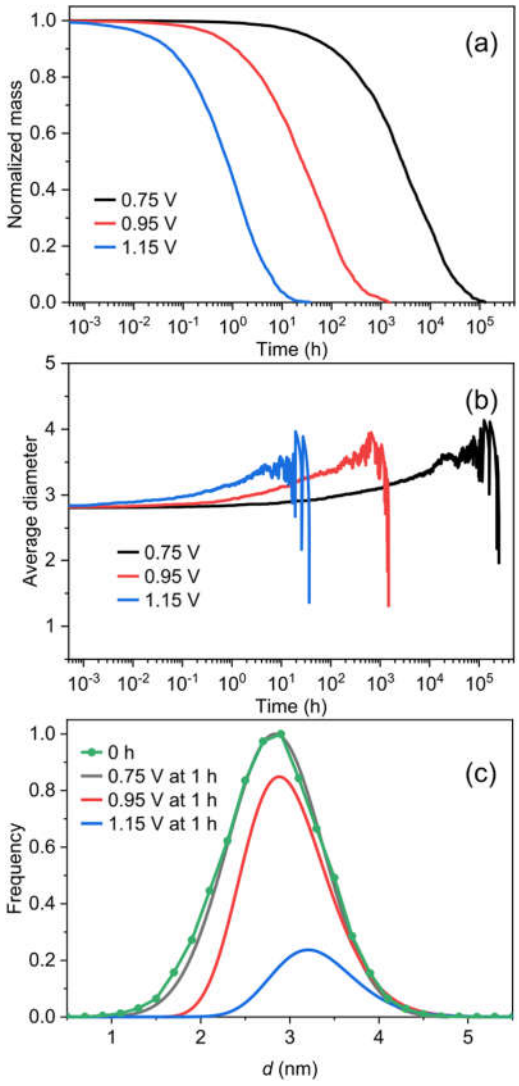

FIG. 6. Influence of the electrode potential on the evolution of (a) the normalized mass, (b) the average diameter, and (c) the normalized particle size distribution of the residual Pt NPs.

of clean Pt at 0.75 V, whereas the process would be slowed down by a factor of five (0.1 h to the same loss of 80%) if the change in surface energies due to oxygen adsorption was included and further slowed down by a factor of 30 (3 h) by taking into account of the increase in standard redox potentials. This result indicates that the redox potential shift plays a more important role on mitigating surface area loss than the change in surface energies. Overall, the chemisorption of oxygen slows down the dissolution of Pt at least 150 times at 1.15 V, in comparison with NPs without considering the oxygen chemisorption.

Such a passivation effect also depends on electrode potentials. While 80% surface area loss of clean NPs takes approximately 0.6 h, 15 h, and 400 h at 1.05 V, 0.95 V, and 0.85 V, respectively, without considering the passivation effect [see Fig. 5(b)], it increases to approximately 16 h, 100 h, and 700 h, respectively, by considering the passivation effect from the oxygen chemisorption. Its influence on the overall dissolution kinetics decreases from a factor of about 27 and 7–2 with a decrease in the electrode potential from 1.05 V and 0.95 V–0.85 V, respectively. Specifically, the suppression effect from the oxygen chemisorption on the kinetics is more significant for faster dissolution at higher potentials.

Figure 6 shows the evolution of the total mass (normalized), the average diameter, and the PSD of NPs with the same initial PSD as above but at different electrode potentials of 0.75 V, 0.95 V, and 1.15 V. It can be found that the normalized mass decreases faster with a gradual increase in the electrode potential from 0.75 V to 1.15 V. Quantitatively, the corresponding half-life time of the mass loss decreases dramatically from 2700, 24 to 0.8 h. Although the passivation effect from the oxygen chemisorption considered here increases with the electrode potential, a rapid increase in the dissolution rate reveals clearly an overwhelming effect of the electrode potential on facilitating the dissolution. Similar results are found for the evolution of the average diameter and the PSD plotted in Figs. 6(b) and 6(c).

The above discussions are based on NPs with an average size of 2.8 nm. To study the size effect, Fig. 7(a) shows the mass loss of NPs with an average diameter of 2.8 nm, 4.8 nm, and 6.8 nm with the same relative standard deviation of 0.2 at 0.85 V. The half-life time of the mass loss is 2.1×10^5 h, 2.3×10^4 h, and 1.9×10^2 h for 6.8 nm, 4.8 nm, and 2.8 nm NPs, respectively. It can be found that the change in half-life time from 4.8 nm to 2.8 nm is more significant than that from 6.8 nm to 4.8. Assuming that the electrochemical catalytic reaction is structurally insensitive, the loss of the mass specific activity would be proportional to the specific surface area plotted in Fig. 7(b). Although the PSD with an initial average size of 2.8 nm having the highest specific surface area among three PSDs is considered, the specific surface area would decrease rapidly by 80% within 900 h. In contrast, the corresponding specific surface area for NPs with an initial average diameter of 4.8 nm and 6.8 nm decreases only by less than 5% and 0.5% at the same period, respectively. Unless the electrochemical catalytic reaction is structurally highly sensitive and has an exceptionally high intrinsic activity at a small size, a careful balance between the high specific surface area and the overall durability of the metal NPs is essential for realistic applications.

In Fig. 7(c), it can be found that the average diameter increases at a wide range of time periods before the steep decrease at a very late stage of dissolution, irrespective of the initial size considered. Nevertheless, the increase in the average size is limited and less than 1 nm in maximum. This is very different from Ostwald ripening, increasing the larger ones at the expense of the smaller ones. Indeed, our previous ripening investigation showed that the increase

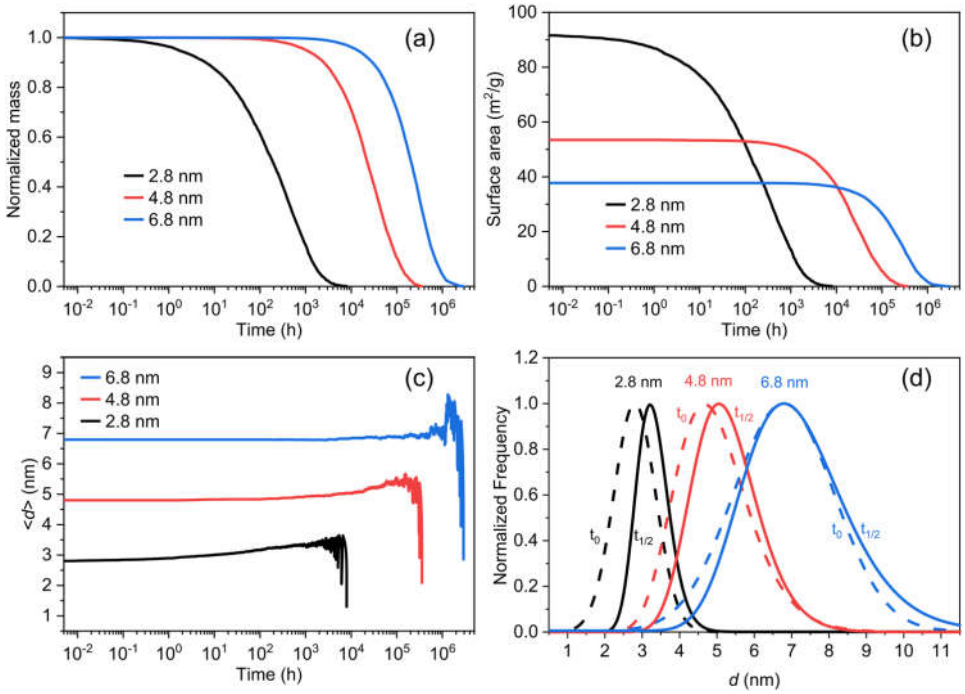

FIG. 7. Influence of the initial average particle size on the evolution of (a) the normalized mass, (b) the ratio of surface area to initial total mass of NPs, and (c) the average diameters of PSD. (d) Normalized PSDs at initial time t_0 and half-time $t_{1/2}$ for the mass loss of 50%.

in the average size is much pronounced, and most importantly, there is no decrease in the average size at all even until the end of ripening.[40]

IV. CONCLUSION

A kinetic theory for the electrochemical dissolution and deposition of the metal nanoparticles was developed. We analyzed the influence of oxygen chemisorption, electrode potential, and particle size on the dissolution of the Pt nanoparticles. We found that while the adsorbed oxygen atoms can stabilize metal NPs and suppress the dissolution by reducing the surface energy and increasing the standard redox potential of dissolution/deposition, the dissolution is dominated and promoted dramatically by the electrode potential. We further found that the dissolution can be offset by increasing the particle size. Thus, a balance of the electrode potential and particle size is crucial for both activity and stability for practical applications.

SUPPLEMENTARY MATERIAL

See the supplementary material for the structures used in the DFT calculation and the corresponding surface adsorption phase diagrams of three Pt facets.

ACKNOWLEDGMENTS

This work was supported by the Key Technologies R&D Program of China (Grant Nos. 2018YFA0208603 and 2017YFB0602205), the National Natural Science Foundation of China (Grant No. 91645202), and the Chinese Academy of Sciences Key Project (No. QYZDJ-SSW-SLH054). Z.Z acknowledges the support from an ECS Toyota Young Investigator Fellowship.

REFERENCES

[1]D. Y. Chung, J. M. Yoo, and Y. E. Sung, Adv. Mater. **30**, 1704123 (2018).
[2]S. Cherevko, N. Kulyk, and K. J. Mayrhofer, Nano Energy **29**, 275 (2016).
[3]L. Li, L. Hu, J. Li, and Z. Wei, Nano Res. **8**, 418 (2015).
[4]Y. Shao-Horn, W. Sheng, S. Chen, P. Ferreira, E. Holby, and D. Morgan, Top. Catal. **46**, 285 (2007).
[5]B. Chakraverty, J. Phys. Chem. Solids **28**, 2401 (1967).
[6]S. Mitsushima, Y. Koizumi, S. Uzuka, and K.-I. Ota, Electrochim. Acta **54**, 455 (2008).
[7]D. J. Myers, X. Wang, M. C. Smith, and K. L. More, J. Electrochem. Soc. **165**, F3178 (2018).
[8]J. Greeley and J. K. Nørskov, Electrochim. Acta **52**, 5829 (2007).
[9]D. Li, C. Wang, D. S. Strmcnik, D. V. Tripkovic, X. Sun, Y. Kang, M. Chi, J. D. Snyder, D. van der Vliet, and Y. Tsai, Energy Environ. Sci. **7**, 4061 (2014).
[10]A. A. Topalov, I. Katsounaros, M. Auinger, S. Cherevko, J. C. Meier, S. O. Klemm, and K. J. Mayrhofer, Angew. Chem., Int. Ed. **51**, 12613 (2012).
[11]S. Hu and W. X. Li, ChemNanoMat **4**, 510 (2018).
[12]J. Wu, W. Gao, H. Yang, and J.-M. Zuo, ACS Nano **11**, 1696 (2017).
[13]H. Schmies, A. Bergmann, J. Drnec, G. Wang, D. Teschner, S. Kühl, D. J. Sandbeck, S. Cherevko, M. Gocyla, and M. Shviro, Adv. Energy Mater. **8**, 1701663 (2018).
[14]A. Kumar and V. Ramani, ACS Catal. **4**, 1516 (2014).
[15]J. C. Meier, C. Galeano, I. Katsounaros, A. A. Topalov, A. Kostka, F. Schüth, and K. J. Mayrhofer, ACS Catal. **2**, 832 (2012).
[16]N. Hodnik, C. Baldizzone, G. Polymeros, S. Geiger, J.-P. Grote, S. Cherevko, A. Mingers, A. Zeradjanin, and K. J. Mayrhofer, Nat. Commun. **7**, 13164 (2016).
[17]H. A. Baroody, D. B. Stolar, and M. H. Eikerling, Electrochim. Acta **283**, 1006 (2018).
[18]P. Urchaga, T. Kadyk, S. G. Rinaldo, A. O. Pistono, J. Hu, W. Lee, C. Richards, M. H. Eikerling, and C. A. Rice, Electrochim. Acta **176**, 1500 (2015).
[19]S. G. Rinaldo, J. Stumper, and M. Eikerling, J. Phys. Chem. C **114**, 5773 (2010).
[20]X. Huang, Z. Zhao, L. Cao, Y. Chen, E. Zhu, Z. Lin, M. Li, A. Yan, A. Zettl, and Y. M. Wang, Science **348**, 1230 (2015).
[21]J. Zhang, K. Sasaki, E. Sutter, and R. Adzic, Science **315**, 220 (2007).
[22]V. R. Stamenkovic, B. Fowler, B. S. Mun, G. Wang, P. N. Ross, C. A. Lucas, and N. M. Marković, Science **315**, 493 (2007).
[23]L. Cao and T. Mueller, Nano Lett. **16**, 7748 (2016).
[24]V. Tripković, I. Cerri, T. Bligaard, and J. Rossmeisl, Catal. Lett. **144**, 380 (2014).
[25]X. Ji, K. T. Lee, R. Holden, L. Zhang, J. Zhang, G. A. Botton, M. Couillard, and L. F. Nazar, Nat. Chem. **2**, 286 (2010).
[26]M. J. Eslamibidgoli, J. Huang, T. Kadyk, A. Malek, and M. Eikerling, Nano Energy **29**, 334 (2016).
[27]S. G. Rinaldo, W. Lee, J. Stumper, and M. Eikerling, Phys. Rev. E **86**, 041601 (2012).
[28]R. M. Darling and J. P. Meyers, J. Electrochem. Soc. **150**, A1523 (2003).
[29]F. Hiraoka, Y. Kohno, K. Matsuzawa, and S. Mitsushima, Electrocatalysis **6**, 102 (2015).
[30]R. K. Ahluwalia, S. Arisetty, X. Wang, X. Wang, R. Subbaraman, S. C. Ball, S. DeCrane, and D. J. Myers, J. Electrochem. Soc. **160**, F447 (2013).
[31]E. F. Holby, W. Sheng, Y. Shao-Horn, and D. Morgan, Energy Environ. Sci. **2**, 865 (2009).
[32]C. Yu, E. F. Holby, R. Yang, M. F. Toney, D. Morgan, and P. Strasser, ChemCatChem **4**, 766 (2012).
[33]J. A. Gilbert, N. N. Kariuki, R. Subbaraman, A. J. Kropf, M. C. Smith, E. F. Holby, D. Morgan, and D. J. Myers, J. Am. Chem. Soc. **134**, 14823 (2012).
[34]M. Matsumoto, T. Miyazaki, and H. Imai, J. Phys. Chem. C **115**, 11163 (2011).
[35]S. Cherevko, A. R. Zeradjanin, G. P. Keeley, and K. J. Mayrhofer, J. Electrochem. Soc. **161**, H822 (2014).
[36]G. Jerkiewicz, G. Vatankhah, J. Lessard, M. P. Soriaga, and Y.-S. Park, Electrochim. Acta **49**, 1451 (2004).
[37]L. Tang, B. Han, K. Persson, C. Friesen, T. He, K. Sieradzki, and G. Ceder, J. Am. Chem. Soc. **132**, 596 (2009).
[38]R. Ouyang, J.-X. Liu, and W.-X. Li, J. Am. Chem. Soc. **135**, 1760 (2013).
[39]Q. Wan, S. Hu, J. Dai, C. Chen, and W.-X. Li, J. Phys. Chem. C **123**, 11020 (2019).
[40]S. Hu and W. X. Li, ChemCatChem **10**, 2900 (2018).
[41]W.-X. Li, C. Stampfl, and M. Scheffler, Phys. Rev. B **68**, 165412 (2003).
[42]W.-X. Li, C. Stampfl, and M. Scheffler, Phys. Rev. Lett. **90**, 256102 (2003).
[43]J. K. Nørskov, J. Rossmeisl, A. Logadottir, L. Lindqvist, J. R. Kitchin, T. Bligaard, and H. Jonsson, J. Phys. Chem. B **108**, 17886 (2004).
[44]J. Rossmeisl, J. K. Nørskov, C. D. Taylor, M. J. Janik, and M. Neurock, J. Phys. Chem. B **110**, 21833 (2006).
[45]Y.-H. Fang and Z.-P. Liu, J. Phys. Chem. C **113**, 9765 (2009).
[46]P. N. Plessow and F. Abild-Pedersen, ACS Catal. **6**, 7098 (2016).
[47]C. T. Campbell, S. C. Parker, and D. E. Starr, Science **298**, 811 (2002).
[48]S. C. Parker and C. T. Campbell, Phys. Rev. B **75**, 035430 (2007).
[49]Z. Zeng and J. Greeley, Nano Energy **29**, 369 (2016).
[50]G. Kresse and J. Furthmüller, Phys. Rev. B **54**, 11169 (1996).
[51]G. Kresse and J. Furthmüller, Comput. Mater. Sci. **6**, 15 (1996).
[52]P. E. Blöchl, Phys. Rev. B **50**, 17953 (1994).
[53]G. Kresse and D. Joubert, Phys. Rev. B **59**, 1758 (1999).
[54]J. P. Perdew, K. Burke, and M. Ernzerhof, Phys. Rev. Lett. **77**, 3865 (1996).
[55]N. Seriani, W. Pompe, and L. C. Ciacchi, J. Phys. Chem. B **110**, 14860 (2006).
[56]H. A. Baroody, G. Jerkiewicz, and M. H. Eikerling, J. Chem. Phys. **146**, 144102 (2017).

[57]T. Zhu, E. J. Hensen, R. A. van Santen, N. Tian, S.-G. Sun, P. Kaghazchi, and T. Jacob, Phys. Chem. Chem. Phys. **15**, 2268 (2013).
[58]E. Antolini, J. Mater. Sci. **38**, 2995 (2003).
[59]P. Ferreira, Y. Shao-Horn, D. Morgan, R. Makharia, S. Kocha, and H. Gasteiger, J. Electrochem. Soc. **152**, A2256 (2005).
[60]Y. Zhou, R. Pasquarelli, T. Holme, J. Berry, D. Ginley, and R. O'Hayre, J. Mater. Chem. **19**, 7830 (2009).
[61]L. Vitos, A. Ruban, H. L. Skriver, and J. Kollar, Surf. Sci. **411**, 186 (1998).
[62]P. Parthasarathy and A. V. Virkar, J. Power Sources **234**, 82 (2013).